Applied Thermal Engineering 233 (2023) 121162

Contents lists available at ScienceDirect

Applied Thermal Engineering

journal homepage: www.elsevier.com/locate/apthermeng

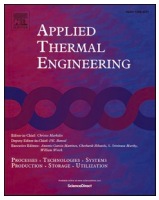

Research Paper

Numerical investigation of the gravity effect on two-phase flow and heat transfer of neon condensation inside horizontal tubes

Fa-Long He [a,c], Wang-Fang Du [a,c,*], Jian-Yin Miao [b,*], Hong-Xing Zhang [b], Si-Xue Liu [b], Chang Liu [b], Jian-Fu Zhao [a,c,*]

[a] CAS Key Laboratory of Microgravity, Institute of Mechanics, Chinese Academy of Sciences, Beijing 100190, China
[b] Beijing Key Laboratory of Space Thermal Control Technology, Institute of Spacecraft System Engineering, China Academy of Space Technology, Beijing 100094, China
[c] School of Engineering Science, University of Chinese Academy of Sciences, Beijing 100049, China

ARTICLE INFO

Keywords:
Condensation flow
Cryogenic working fluid
Gravity effect
Two phase flow pattern

ABSTRACT

The condensation flow and heat transfer characteristics of cryogenic neon inside horizontal tubes with diameters of 1 mm and 2 mm were numerically investigated. The mass flux ranged from 20 to 187 kg/(m^2·s) for gravity levels includes zero gravity, Lunar gravity, Martian gravity, and Earth gravity. The effects of gravity on the condensation flow pattern, local condensate film distribution, and local and global heat transfer were analyzed in detail. The gravity effect on the condensation heat transfer showed three states, including enhancement, deterioration and gravity-independence, which were mainly determined by the mass flux and vapor quality. Under normal gravity, the condensation heat transfer coefficients increased with increasing mass flux and decreasing tube diameter. Under low mass flux, the cryogenic neon underwent enhanced condensation heat transfer under zero gravity and reduced gravity in the high vapor quality region but deteriorated condensation heat transfer in the low vapor quality region. By increasing the mass flux, the gravity effect was effectively suppressed, which resulted in gravity-independent behavior of condensation heat transfer in the high vapor quality region. The gravity effect significantly affected the liquid film distribution in the condensation process, with a more uniform distribution of the liquid film appearing along the circumferential direction as the gravity level decreased. However, due to the low surface tension of the deep cryogenic fluid, the condensation interface was more prone to flow instability under reduced gravity levels.

1. Introduction

As an important component of two-phase thermal management systems, condensers have been widely implemented in multiple industries, such as heating, ventilation, air conditioning, and refrigeration (HVAC&R) systems on the ground and thermal control systems for spacecraft. As space-based exploration and utilization are projected to increase greatly in exploration depth, the working temperature control range and space tolerability of systems require increases in stable and efficient thermal control technologies suitable for the cryogenic temperature range. In this regard, cryogenic two-phase thermal control technology has garnered significant attention, as it offers high heat transfer efficiency and the potential for effective weight reduction. Despite these advantages, the changing gravity level and cryogenic working fluid thermophysical properties also pose significant challenges, including instability at the vapor–liquid interface resulting from the lower surface tension of cryogenic working fluid and changes in vapor–liquid two-phase flow and heat transfer characteristics under microgravity level. These issues must be carefully addressed to realize the full potential of cryogenic two-phase thermal control technology for space applications.

Condensation flow and heat transfer are important physical processes in two-phase thermal control systems. The flow and heat transfer performance during condensation play a crucial role in the design of two-phase thermal management systems, due to determining the heat transfer efficiency and operating stability of the system. A tube containing condensation flow is considered to be the most suitable configuration for space applications. [1] In fact, the high condensation flow stability and heat transfer coefficients commonly achieved in condensers

* Corresponding authors at: CAS Key Laboratory of Microgravity, Institute of Mechanics, Chinese Academy of Sciences, Beijing 100190, China (W.F. Du and J.F. Zhao) and Beijing Key Laboratory of Space Thermal Control Technology, Institute of Spacecraft System Engineering, China Academy of Space Technology, Beijing 100094, China (J.Y. Miao).
E-mail addresses: duwangfang@imech.ac.cn (W.-F. Du), miaojianyin@sina.com.cn (J.-Y. Miao), jfzhao@imech.ac.cn (J.-F. Zhao).

https://doi.org/10.1016/j.applthermaleng.2023.121162
Received 26 February 2023; Received in revised form 6 June 2023; Accepted 13 July 2023
Available online 14 July 2023

Nomenclature

Bo	Bond number
Fr	Froude number
Re	Reynolds number
d	tube diameter (mm)
g	acceleration of gravity (m/s^2)
G	mass flux (kg/(m^2·s))
E	specific internal energy (kJ/kg)
k	thermal conductivity (W/(m·K))
h	specific enthalpy (kJ/kg)
Δh	latent heat of evaporation (kJ/kg)
v	gas velocity (m/s)
P	pressure (Pa)
T	temperature (K)

Greek symbols

α	volume fraction (~)
β	phase change accommodate factor
μ	dynamic viscosity (Pa•s)
ν	kinematic viscosity (m^2/s)
ρ	density (kg/m^3)
σ	surface tension (N/m)
κ	turbulent kinetic energy (J)
ω	specific dissipation rate

Subscripts

cr	critical
d	droplet
e	earth
s	surface tension
sg	superficial gas
sat	saturated state
l	liquid phase
v	vapor phase
t	turbulence
lo	liquid only

are direct results of the complicated interface transport, which is usually determined by inertial forces, surface tension and gravity. However, limited by cryogenic temperature and microgravity conditions, there are few reports on condensation flow in tubes under such conditions. Commonly, experiments are carried out with a working fluid at normal temperature or under normal gravity. Moreover, early studies of microgravity two-phase flow mainly studied the flow pattern and pressure drop under adiabatic conditions using air–water as the working fluid. As a result, the design of flow and heat transfer performance in condensers depends mainly on empirical correlation formulas for normal temperature working fluids achieved from these terrestrial experiments. Although early studies accumulated many achievements and inspired methods for subsequent research on flow condensation and boiling, most results considering adiabatic two-phase flow seem to be not applicable to condensation flow. Therefore, a detailed analysis of the effects of different forces on vapor–liquid behavior and heat transfer performance in the flow condensation process is of paramount significance to the optimization and design of condensers, especially those used for space applications.

1.1. The influence of gravity on flow condensation

Currently, a great deal of work has been conducted to study the flow pattern, heat transfer and pressure drop of condensing flow, but most of this experimental research is carried out in the ground environment due to the limited availability of microgravity-based systems. To investigate the impact of gravity on condensation flow, a straightforward and effective approach involves analyzing the effects of altering the gravity direction on condensation flow under a ground gravity environment. Another method for condensation flow experiments under Earth gravity level is to reduce the channel size, enhance heat transfer and suppress the effects of gravity. Therefore, studying the flow and heat transfer of condensation and boiling in micro/mini tubes has long been a crucial research area in two-phase thermal control systems. The present work mainly focuses on the effect of gravity on condensation. For more detailed discussions of micro/mini tube condensation research to enhance heat transfer, please refer to Reference [2].

To investigate the effect of gravity on condensation, Wang and Du [3] presented a theoretical and experimental study on downward flow of water vapor condensation in tubes with different orientations. The experimental tube's inner diameter ranges from 1.94 mm to 4.98 mm, the inclination angle range is 0°-45° and the mass flux range is 11.3–94.5 kg/(m^2·s). Based on the analytical and experimental results, the local Nusselt number of condensation flow was increased or decreased with the inclination angle depending on the tube diameter, vapor quality and mass flux. They explained these results as the effect of gravity on the thickness of the condensate film.

Lips and Meyer [4] presented experimental studies of the R134a condensation flow pattern and heat transfer coefficient through an 8.38 mm inner tube diameter in different incline angles considering the range from vertical downward to vertical upward flow. The image results showed that the influence of tube inclination on the flow pattern is strongly dependent on the vapor quality and mass flux. For high vapor qualities or mass fluxes, the flow pattern is annular and insensitive to the inclination angle, but for low vapor qualities or mass fluxes, the flow pattern is dependent on the inclination angle. For low vapor qualities or low mass flux conditions, the condensation heat transfer results indicated that there is an optimum inclination angle (between −15° and −30°) corresponding to the maximum heat transfer coefficient for downward flow, and a worst inclination angle (approximately 15°) corresponding to the minimum heat transfer coefficient for upward flow. The experiments of Bortolin et al. [5] for micro/mini tube condensation yielded similar results. In their experiment, the flow condensation of R134a inside a square tube with a hydraulic diameter of 1.23 mm was investigated. The flow directions included horizontal, vertical upward and vertical downward flow. The results showed that the condensation heat transfer coefficient was not sensitive to the flow direction at a mass flux of 390 kg/(m^2·s). The condensation heat transfer coefficient of vertical downward flow was lower than that of horizontal and vertical upward flow for vapor quality lower than 0.6 at a mass flux of 135 kg/(m^2·s). The authors explained that the downward flow might enhance the two-phase flow stability, which acted to present the annular flow region with a thicker liquid film and limit the slug and plug flow pattern. To a certain extent, this also indicated that the effect of gravity can either enhance condensation heat transfer or degrade it.

Park et al. [6] performed a series of experimental studies of condensation of FC-72 in a circular tube with an 11.89 mm diameter for horizontal flow, vertical downward, and vertical upward flow to assess the gravity effects on the flow condensation flow pattern and heat transfer coefficients. The two-phase flow images for different orientations showed that the liquid film behavior differences occurred only at relatively low mass fluxes, with horizontal flow exhibiting stratification, vertical downward flow exhibiting annular flow, and vertical upward flow exhibiting falling film behavior. The heat transfer coefficient measurements showed that gravity enhanced condensation heat transfer for vertical downward flow, or it deteriorated condensation heat transfer

for vertical upward flow. With the increase in the mass flux, the gravity effect on the flow pattern and the condensation heat transfer was weakened due to the inertial force being strengthened. It should be noted that as the inlet mass flux increased, the schlieren fluctuations on the upper wall of the horizontal tube in the condensing flow changed from smooth to rough, and distinct liquid film breakage, liquid strip pulling, and droplet entrainment occurred at the interface of the bottom liquid film. When combined with the heat transfer coefficient data at different mass fluxes, it is evident that increasing the vapor-phase mass velocity at the inlet of the condensation flow will amplify the disturbance of the flow to the vapor–liquid interface of annular and stratified flows, thereby enhancing the heat transfer efficiency to some extent. As the secondary part of this study, O'Neill et al. [7] developed mechanistic criteria for inclination angle-based flow condensation that was gravity-independent. The condition criteria was expressed in terms of relevant dimensionless groups, including the Froude, Reynolds, Bond and Weber numbers. As a follow-up study, O'Neill et al. [8] investigated the condensation flow of FC-72 in a smaller diameter tube (7.12 mm) in different orientations. Similar conclusions were drawn regarding the effects of mass flux, vapor quality and orientations on condensation heat transfer as compared to their previous studies. Notably, the parametric trend analysis for condensation heat transfer highlighted the significant impact of mass flux, with vapor quality being the next most significant factor.

The aforementioned experimental studies on the inclination angle and flow direction of the under normal gravity indicate that the effect of gravity on the condensation heat transfer should not be ignored, especially under small mass flux and low vapor quality conditions. In fact, the implicit and explicit effects of gravity are determined by the local competition of forces on the liquid film in the two-phase system under forced convective flow. For a specific working condition, a change in gravity level or direction will eventually lead to a change in the force state of the liquid film, but the influence of this change on the two-phase flow and heat transfer mainly depends on the resulting force state driving the local liquid film movement. When the vapor and liquid are mainly driven by inertial forces, gravity and surface tension effects might be suppressed. When the motion of the vapor and liquid film is driven by gravity or buoyancy, the gravity effect is significant in two-phase flow.

Compared with the experimental study of condensation under normal gravity, the experimental study of condensation under a microgravity environment is very rare, due to the scarcity of microgravity experimental resources as a result of their high cost. Lebaigue et al. [9] conducted microgravity condensation flow experiments aboard sounding rocket MASER-9 and obtained six sets of effective condensation heat transfer experimental data. In this experiment, a pumped two-phase loop was adopted, ammonia was used as the working fluid, and the tube was made of aluminum with an inner diameter of 4.8 mm. The maximum heat load was 150 W, and the maximum flow rate was about 24 kg/(m^2·s). Comparing the obtained microgravity condensation flow heat transfer coefficient with several commonly used condensation heat transfer models, the results showed that the classical model could not correctly predict the condensation heat transfer coefficient under microgravity conditions, and there were even differences of magnitude. However, it was not possible to determine the effect of gravity on flow condensation because there was no controlled ground experiment.

Kawasaki et al. [10] reported the test results of condenser operation in a reservoir-embedded loop heat pipe (LHP) system on the KIKU-8 test satellite in Japan. The condenser was an aluminum snake pipe with an inner diameter of 4.5 mm and a total length of 5.5 m, which was implanted in the expanded radiator. The maximum heat load reached 400 W, the working fluid was ammonia, and the operating temperature range was − 40 to 60 °C. The experimental results show that the length of the two-phase zone does not change with the heat load and is close to that of complete condensation under normal gravity. Under space microgravity conditions, the length of the two-phase region increases with increasing heat load and is equal to the length of the condenser at high heat flux. However, when the heat load is low, the two-phase zone is shorter in space microgravity than on the ground, which reflects the enhanced heat transfer. Under the condition of a high heat load, the steam cannot be completely condensed in the space environment, and the outlet of the condenser is still in a two-phase state, which reflects that the heat transfer deteriorates.

As a prelude to NASA's development of the Flow Boiling and Condensation Experiment (FBCE) for the International Space Station (ISS), Li et al. [11,12] performed annular flow condensation studies of FC-72 inside a smooth 7.12 mm inner diameter tube under microgravity and reduced gravity in parabolic flight experiments. The mass flux of FC-72 ranged from 129 to 340.5 kg/(m^2·s), and the saturation temperature range was 60–63.4℃. The experimental results of the microgravity annular flow pattern under different mass fluxes showed that the mass flux rate presents a great influence on the condensate film morphology. At lower mass flux, the liquid film under microgravity was smooth and laminar, and with increasing mass flux, the liquid film showed obvious multiscale ripple and turbulence. Compared with the annular flow patterns under different gravity levels, the effect of gravity on the morphology of the liquid film was more obvious only under the low mass flux condition. With the increase in gravity level, the thickness of the liquid film at the bottom of the tube was significantly thicker.

Recently, experimental parabolic flight microgravity data were collected by Azzolin et al. [13,14] corresponding to flow condensation of HFE-7000 inside a 3.38 mm inner diameter channel with a mass flux range of 30–170 kg/(m^2·s). The flow pattern visualizations showed that the condensate film as thicker at the bottom and not visible at the top of the tube under both normal gravity and hyper gravity. Under microgravity conditions, the liquid film tended to spread along the inner circumference of the tube, while interfacial waves of varying sizes rippled across the phase interface. As the mass flux increased, the interface became more disrupted. A comparison of the condensation heat transfer coefficients between microgravity and normal gravity revealed a striking contrast in the effects on heat transfer. Under normal gravity, the heat transfer process was strengthened, while under microgravity, the heat transfer rate was deteriorated, especially under lower mass flux. This phenomenon can be mainly attributed to the influence of gravity on the liquid phase distribution within the condensation channel, which in turn affects the heat transfer mechanism during the condensation process. Furthermore, the degree of heat transfer enhancement is closely related to the mass flux, with the shear stress of the vapor acting on the liquid film becoming the dominant factor in the condensation process as the mass flux increases. Consequently, the influence of gravity on the condensation heat transfer weakens.

It should be noted that achieving a steady state in condensation flow takes a relatively long time and thus requires a longer microgravity period. However, the microgravity time provided by parabolic aircraft is only approximately 20 s. To reduce the experimental response time, specific measures must be implemented, such as maintaining a consistent flow rate of the condensing working fluid and ensuring supercooling of the walls. Hence, the acquired condensation flow and heat transfer data through parabolic aircraft necessitate meticulous evaluation and analysis.

1.2. The condensation flow of the cryogenic working fluid

Similar to the limited resources of microgravity experiments, the condensation flow of working fluids under cryogenic temperature also requires extremely strict experimental conditions to accurately measure the pressure drop, temperature and flow pattern. Therefore, experimental studies of condensation flow and heat transfer of cryogenic working fluids are much less prevalent than that for normal temperature working fluid. Qi et al. [15,16] designed a set of experimental observation platforms for cryogenic temperature condensation flow and experimentally studied the heat transfer coefficient, friction pressure

drop and flow pattern observation results during the condensation flow of nitrogen working fluid. The experiments were conducted at saturation temperatures ranging from 101.0 to 106.6 K, with mass fluxes ranging from 13.1 to 78.6 kg/(m^2·s) for a 2 mm tube and from 52.4 to 314.0 kg/(m^2·s) for a 1 mm tube. The observation results show that the horizontal two-phase flow patterns in the condensation flow process of nitrogen working fluid are mainly annular flow, stratified flow and bubble flow. The condensation heat transfer coefficient data of horizontal and vertical downward flow were obtained. For a 2 mm diameter tube, the horizontal flow condensation heat transfer coefficient was higher than the vertical downward flow under the same conditions, especially at lower mass flux. As the mass flow rate increased, the difference between the two decreased. However, for a 1 mm diameter tube, even at higher mass flux, the horizontal flow condensation heat transfer coefficient was still higher than the vertical downward flow, especially in the high vapor quality region.

Using the same cryogenic testing platform, Qi [17] conducted condensation flow experiments with neon as the working fluid in 1 mm and 2 mm inner diameter tubes, and the experimental saturation temperature was approximately 37.5 K. The heat transfer coefficient and pressure drop of the neon condensation flow in these small diameter tubes were obtained. The results showed that the tube diameter imparted a significant impact on the condensation heat transfer coefficient and reducing the tube diameter enhanced the condensation heat transfer. However, due to the temperature limitations of the visualization equipment, the condensation flow pattern of neon was not obtained, and the discussion of the flow pattern was only based on the results acquired with nitrogen as the working fluid. However, because there is an order of magnitude difference in the surface tension between nitrogen and neon, the flow pattern analysis model that they applied may not be applicable.

The condensation flow and heat transfer results of the cryogenic working fluid show that the correlations of the heat transfer coefficient and friction pressure drop established based on the experimental data using normal temperature working fluid cannot achieve accurate prediction for a cryogenic working fluid. This is mainly caused by the difference in the thermophysical properties of the working fluid. The low latent heat of vaporization and the small surface tension of the cryogenic temperature working fluid may lead to a large change in the vapor–liquid two-phase flow heat transfer characteristics during the flow condensation or boiling.

1.3. Numerical simulation of flow condensation

Compared to experimental research, numerical simulation can capture more physical parameters that are difficult to observe in detail in experiments. It is therefore widely used in scientific research. Currently, the primary simulation methods for condensation include the Volume of Fluid (VOF) method, the Euler two-fluid model, and the mixture model [18]. Among these, the VOF method has gained widespread popularity due to its capability to capture the clear vapor–liquid interface and the dynamics of the interface behavior with remarkable precision. As such, it has become the favored simulation method for investigating flow condensation processes.

Da Riva and Del Col [19] used the VOF method to simulate and analyze the effects of gravity during the condensation of R134a in a 1 mm inner diameter tube. Their simulation results showed that the condensation heat transfer process is dominated by gravity at lower mass fluxes, whereas the influence of gravity is negligible at higher mass fluxes. The effect of surface tension on flow condensation was analyzed, and the results indicated that it surface tension showed an insignificant impact on the heat transfer coefficient. Neglecting surface tension even enhanced heat transfer (to some degree) at lower vapor quality ranges. Furthermore, the authors compared the heat transfer coefficients of vertical downward flow condensation and horizontal condensation under normal gravity and found significant differences between the two, with the former being significantly lower than the latter in the lower range of vapor quality. Prior, Riva et al. [20] performed a detailed analysis comparing the effects of laminar and turbulent liquid film models on the calculation of condensation heat transfer coefficients. The results showed that at high mass fluxes, the laminar liquid film model significantly underestimated the condensation heat transfer coefficient, and the condensation heat transfer coefficient values corresponding to different quality conditions were very similar. However, at low mass fluxes, the liquid film turbulent model overestimated the experimental values. This provides an important reference for setting up turbulent models in condensation flow simulations.

Li et al. [21] numerically investigated the heat transfer characteristics of R410A condensation in horizontal tubes with an inner diameter of 3.78 mm under normal and reduced gravity. The results showed that at a lower mass flux, increasing the gravity level leads to an increase in heat transfer coefficients, while differences under varying gravity levels are insignificant at higher mass fluxes. The liquid film thickness decreases with increasing gravity at the top of the tube, while the average liquid film thickness is nearly the same under different gravity levels for the same vapor quality and mass flux. Local heat transfer coefficients increase with increasing gravity at the top of the tube and decrease with increasing gravity at the bottom. The relative proportion of the thin liquid film region with respect to the entire channel is thus crucial for determining the overall heat transfer coefficients in condensing flow.

Wen et al. [22] conducted a simulation analysis of circular tube condensation of R1234ze(E) in the range of tube diameters from 0.493 to 4.57 mm using the VOF model. The simulation results showed that a decrease in tube diameter would significantly reduce the liquid film thickness, and the effects of gravity on the liquid film and velocity distribution would result in a combined effect, leading to both enhanced and deteriorated heat transfer during the condensation process. Gu et al. [23] achieved similar results in their numerical studies of the condensation characteristics of R1234ze(E) inside an inclined circular tube with a diameter of 4.57 mm. The simulation results showed that the inclination angle had a negligible effect on heat transfer coefficients at high mass fluxes and vapor qualities, but could cause an increase or decrease in heat performance when decreasing the mass flux and vapor quality. Additionally, at the same inclination angle, slightly higher heat transfer coefficients were observed for vertical downward flow.

The above models were all based on steady-state calculations and thus cannot accurately describe dynamic behaviors in flow and condensation, such as intermittent flow and slug flow. Additionally, the steady-state solution method ignores the dynamic behavior of the vapor–liquid interface, which has an important impact on the process of condensation flow and heat transfer. Ganapathy et al. [24] used a two-dimensional transient model to simulate the flow and heat transfer characteristics during R134a condensation in a 0.1 mm diameter tube, obtaining the flow condensation pattern. By comparing the two-phase friction pressure drop and Nu number correlation, the predictive accuracy of the model was evaluated. Lei et al. [25] established a three-dimensional transient simulation model of FC-72 flow condensation in a 1 mm square tube and analyzed in detail the effects of turbulence intensity and mass transfer intensity on the simulation results based on experimental data. The reliability of the model was verified by comparing simulated and experimental data on the wall temperature.

It is obvious that the transient simulation analysis is less than the steady-state simulation. This is mainly due to the time consuming and low efficiency of transient simulation. For this problem, conventional computational fluid dynamics (CFD) methods do not have a suitable solution. However, with the development of machine learning and intelligent algorithms, new efficient and accurate computing methods will be developed. Machine learning method is one of the effective methods to deal with complicated transient problems. With the help of machine learning method [26,27], the time-consuming problem of traditional CFD transient calculation can be effectively reduced on the premise of ensuring calculation accuracy. In conclusion, the above

studies fully demonstrate the feasibility of simulating flow condensation phenomena through numerical analysis.

1.4. Objectives of the present study

Based on previous experimental and simulation studies on the effects of pipe inclination and gravity orientation on flow condensation, we determined that the gravitational effect strongly depends on the mass flux, vapor quality, and two-phase flow pattern. However, most condensation flow studies are focused on room temperature working fluids, such as R134a and R1234ze(E). Due to experimental limitations, the study of flow patterns and heat transfer coefficients in the condensation flow of cryogenic working fluids is still very limited. Moreover, previous experimental studies have shown that the condensation flow and heat transfer characteristics of cryogenic working fluids are significantly different from those of room temperature working fluids. Therefore, it is necessary to carry out detailed numerical simulation studies on the condensation flow and heat transfer performance of cryogenic working fluids to better understand the flow and heat transfer performance and the influence of gravity on cryogenic condensation flow. In the present work, the condensation flow and heat transfer characteristics of neon working fluid are numerically investigated inside 1 mm and 2 mm diameter tubes under different conditions. The numerical model was validated by flow condensation heat transfer coefficient experimental data of a neon working fluid. The effects of tube diameter, mass flux, and gravity level on flow condensation patterns, heat transfer coefficients, and local liquid film distribution characteristics were discussed. This study aims to provide new insights into the analysis of the effects of gravity on cryogenic condensation flow and heat transfer. The related research will help guide the design and optimization of cryogenic condensers under different gravity levels.

2. Numerical models

The VOF model proposed by Hirt and Nichols [28] is used in this simulation to calculate the phase distribution during the condensation process, combined with an interface reconstruction algorithm to capture the interface behavior. The basic assumptions of the current VOF model include the following:

(1) The vapor and liquid phases are incompressible fluids.
(2) The physical properties of the working fluid, including density, specific heat capacity, surface tension, and latent heat of vaporization are constant for a certain saturation temperature.
(3) The nonequilibrium thermodynamic effects are ignored during the phase change process. Mass transfer between the vapor and liquid phases only occurs at the interface, which indicates that the condensation process can only occur in the two-phase region.
(4) Interfacial shear velocity is ignored, which indicates that the vapor and liquid phase velocities are the same for the two-phase control volume.
(5) The influence of buoyancy-driven convection on turbulence is neglected.

2.1. The VOF model

The calculation of the vapor–liquid interface in the VOF model is obtained using the continuity equation for the volume fraction of the vapor and the liquid phase. The unsteady continuity equation of the volume fraction is shown in the following equation:

$$\frac{\partial}{\partial t}(\alpha_v \rho_v) + \nabla \cdot \left(\alpha_v \rho_v \overrightarrow{v}_v \right) = \left(\dot{m}_{l-v} - \dot{m}_{v-l} \right) \tag{1}$$

where α is the volume fraction of the vapor phase, ρ is the density, and the subscripts l and v denote the liquid phase and vapor phase, respectively. $\dot{m}_{l\text{-}v}$ is the mass transfer intensity from the liquid to vapor phase, whereas $\dot{m}_{v\text{-}l}$ is the mass transfer intensity from the vapor to liquid phase. The calculation of mass transfer intensity during phase change will be discussed in detail in the phase change model section.

The above equation can be used to calculate the volume fraction of the control volume. The mixture density of the control volume is calculated using the following equation:

$$\rho = \alpha \rho_v + (1 - \alpha) \rho_l \tag{2}$$

It should be noted that not only is the mixture density of the control volume calculated using the above method, but other physical properties inside the control volume are also determined in the same form. The viscosity and thermal conductivity in the control volume are defined as follows:

$$\mu = \alpha \mu_v + (1 - \alpha) \mu_l \tag{3}$$

and

$$k = \alpha k_v + (1 - \alpha) k_l \tag{4}$$

Since the interphase velocity difference inside the control volume is ignored, only one set of momentum equations is needed to describe the change in momentum inside the control volume. The following equation describes the unsteady momentum:

$$\frac{\partial}{\partial t}(\rho \overrightarrow{v}) + \nabla \cdot (\rho \overrightarrow{v} \overrightarrow{v}) = -\nabla P + \nabla \cdot [\mu (\nabla \overrightarrow{v} + \nabla \overrightarrow{v}^T)] + \rho \overrightarrow{g} + \overrightarrow{F}_s \tag{5}$$

where ρ, v, P, μ, g and F_s are the mixture density, velocity, local pressure, mixture viscosity, gravity acceleration and surface tension force,

Table 1
The condensation phase transfer intensity factor value.

Year	Author	Working fluid	Condition	γ_c
2011	Da Riva et al.	R134a	G = 100–800 kg/(m^2·s)	7.5×10^5 –1 $\times 10^7$
2012	Liu et al.	Water	T_{sat} = 40 °C u_{in} = 1–3 m/s	5000
2013	Bortolin et al.	R134a	T_{sat} = 100 °C G = 400–800 kg/(m^2·s)	1×10^6 –5 × 10^6
2014	Chen et al.	FC-72	T_{sat} = 40 °C G = 68–150 kg/(m^2·s)	33,000
2015	Lee et al.	FC-72	T_{sat} = 60 °C G = 184.4–459 kg/(m^2·s)	10,000
2016	Kharangate et al.	FC-72	T_{sat} = 63.5–86.6 °C G = 58.4–271.5 kg/(m^2·s)	10,000
2017	Li et al.	R410a	T_{sat} = 69.05–74.55 °C G = 426–1026 kg/(m^2·s)	1.5×10^6
2018	Wu and Li	R32	T_{sat} = 47 °C G = 100–200 kg/(m^2·s)	3.33×10^9
2019	Gu et al.	R1234ze(E)	T_{sat} = 40–50 °C G = 400–800 kg/(m^2·s)	8×10^5 –3 × 10^6
2020	Lei et al.	FC-72	T_{sat} = 40 °C G = 68–367 kg/(m^2·s) T_{sat} = 57.2–62.3 °C	33,000

respectively. The surface tension force plays a crucial role in condensation within microchannels. To determine this term, the continuum surface force (CSF) model developed by Brackbill et al. [29] was utilized:

$$\overrightarrow{F}_s = \frac{\rho\sigma\nabla\alpha_l}{0.5(\rho_l+\rho_v)}\nabla\cdot\frac{\nabla\alpha_l}{|\nabla\alpha_l|} \tag{6}$$

Similarly, since the convective heat transfer between the two phases inside the control volume is ignored, only one set of energy equations is needed to describe the energy exchange between the control volume and the outside world. The unsteady energy conservation equation is given as follows:

$$\frac{\partial}{\partial t}(\rho E)+\nabla\cdot[\overrightarrow{v}(\rho E + P)] = \nabla\cdot[k(\nabla T)]+\left(\dot{m}_{l-v}-\dot{m}_{v-l}\right)\Delta h \tag{7}$$

where E, T and $\triangle h$ are the specific internal energy (energy per unit mass), temperature and latent heat of evaporation, respectively. The mixture-specific internal energy is expressed as:

$$E = \frac{\alpha\rho_v E_v+(1-\alpha)\rho_l E_l}{\alpha\rho_v+(1-\alpha)\rho_l} \tag{8}$$

In the above equation, the vapor phase-specific internal energy is defined as:

$$E_v = h_v - \frac{P}{\rho_v}+\frac{v^2}{2} \tag{9}$$

where h_v is the specific heat of the vapor phase. The liquid phase-specific internal energy is determined in a similar way.

2.2. Turbulence model

In the process of flow condensation, turbulent effects play a crucial role, and the turbulent states of each phase directly impact the flow and heat transfer performance during condensation. In this numerical study of neon flow condensation, the Reynolds number (Re_{lo}) of the fully liquid phase of the working fluid in different pipe diameters reaches orders of magnitude ranging from 10^3 to 10^4. Therefore, it is necessary to consider the influence of turbulence. The Shear–Stress Transport (SST) κ-ω model [30] has been widely used in previous simulation studies on condensation and is considered to effectively describe the turbulent effects in the condensation process. The turbulent kinetic energy and specific dissipation rate in the SST κ-ω model can be described by the following transport equations:

$$\frac{\partial}{\partial t}(\alpha\rho\kappa)+\nabla\cdot(\alpha\rho\overrightarrow{v}\kappa) = \nabla\cdot(\alpha\rho\Gamma_k\nabla\kappa)+\mu_t S^2-\rho\beta^*\kappa\omega+G_b \tag{10}$$

$$\frac{\partial}{\partial t}(\alpha\rho\omega)+\nabla\cdot(\alpha\rho\overrightarrow{v}\omega) = \nabla\cdot(\alpha\rho\Gamma_\omega\nabla\omega)+\frac{a}{\upsilon_t}\mu_t S^2-\rho\beta\omega^2+2(1-F_1)\rho\frac{1}{1.168\omega}\nabla\kappa\nabla\omega+G_{\omega b} \tag{11}$$

where κ, ω, μ_t, S and ν_t are the turbulent kinetic energy, specific dissipation rate, turbulent viscosity, strain rate magnitude and turbulent kinematic viscosity, respectively. Γ_κ and Γω represent the effective diffusivity of turbulent kinetic energy and specific dissipation rate, respectively. G_b and $G_{\omega b}$ account for buoyancy terms. α, β and F are the coefficients of the model.

2.3. Phase change model

Among these phase change models, the Lee model [31] has gained widespread popularity due to its relatively clear physical meaning and relatively simple expression at the macroscopic level: when the vapor phase temperature is lower than the saturation temperature, the vapor phase condenses; otherwise, the liquid phase evaporates. As such, it has become the favored method for the description of phase change processes. The formula is expressed in the following form:

$$\begin{cases} m_{1-v} = \gamma_e * \alpha_l\rho_l\dfrac{(T_l-T_{sat})}{T_{sat}} evaporation T_l > T_{sat} \\ m_{1-v} = \gamma_e * \alpha_v\rho_v\dfrac{(T_{sat}-T_v)}{T_{sat}} evaporation T_v < T_{sat} \end{cases} \tag{12}$$

where ρ is the density, T is the temperature, and α is the volume fraction. The subscripts l, v, and sat denote the liquid phase, vapor phase, and saturation, respectively. $\dot{m}$ is the mass transfer rate of phase change per unit volume, γ is the adjustment factor of phase change mass transfer intensity or frequency of phase change, and the subscripts e and c denote evaporation and condensation, respectively.

In fact, the Lee model is deduced from the Hertz-Knudsen and Clausius-Claperyon equation by introducing the interface area density model. The phase change intensity factor is a function of the properties and some model parameters, such as the bubble or droplet diameter and the phase change accommodation factor. For condensation, the phase change intensity factor is expressed as follows:

$$\gamma_c = \frac{6\Delta h}{d_d}\beta\sqrt{\frac{M}{2\pi RT_{sat}}}\left(\frac{\alpha_l\rho_l}{\rho_l-\rho_v}\right) \tag{13}$$

where β denotes the phase change accommodation factor, which is commonly used to characterize the thermodynamic nonequilibrium of the phase transition process. When β = 1, the phase change process is in a state of thermodynamic equilibrium. The equivalent diameter, d_d, is dependent on the configuration of the interface surface density. For the symmetric interfacial area density model, d represents the diameter of the condensed liquid nucleus, although it is challenging to assign a precise value to this parameter.

The phase change mass transfer intensity factor is subject to influences such as the working fluid, grid, and operating conditions, making it difficult to determine a universal value for this factor. The condensation mass transfer intensity factor exhibits a broad range of values. However, for condensation simulations, this value is often assigned a relatively large order of magnitude. Table 1 presents the values of the phase change mass transfer intensity factor used in some previous condensation flow simulations. Riva et al. [3] used a range of values of 10^5 to 10^7 when calculating R134a condensation, whereas Lei et al. [7] set this value to 33,000 after comparing the wall temperature of FC-72 condensation experiments. Methods for determining the phase change intensity factor include comparison with experimental data, controlling the interface temperature difference to approximately 1 K, and utilizing empirical values. Based on numerical simulation, setting the mass transfer intensity to a small value might cause a large temperature jump, while setting it to a large value might pose a challenge for ensuring simulation convergence. In this simulation study, setting the mass transfer intensity factor to 30,000 resulted in a deviation of approximately 1 K between the interface temperature and the saturation temperature while ensuring favorable convergence.

2.4. Solution method

The condensation flow simulation adopts the transient solution method by using ANSYS FLUENT [32]. The transient term in the equation adopts the first-order implicit scheme. The VOF equation is solved by the explicit difference method, and the Courant number is set to the range of 0.25–0.5. The interface capture method is the geometric reconstruction algorithm (Geo-Reconstruct). The Pressure-Implicit with Splitting of Operators (PISO) is used for speed and pressure coupling equations, and the PRESTO! (PREssure STaggering Option) algorithm is used to determine the pressure difference. The gradient of variables is calculated using the element-based Green-Gauss algorithm. The momentum and energy equations are discretized by a second-order upwind difference scheme, and the turbulent kinetic energy and specific dissipation equations are discretized by a first-order upwind difference scheme.

3. Model validation

3.1. Computational domain and boundary conditions

In this simulation, a planar symmetry tube is used to model flow condensation in a horizontal microtube to reduce the computational resources and time. Fig. 1 shows the basic configuration of the horizontal tube. All these simulation results concern neon condensation flow. The saturation temperature of neon ranges from 24.5 to 44.5 K, which is relatively low. The main thermophysical properties for neon at the corresponding temperature are obtained from the NIST Standard Reference Database REFPROP-v9.0 tool [33]. The condensing flow of the neon working fluid at saturation temperatures of 34.5 K and 37.5 K are used. The thermophysical properties corresponding to the saturation temperatures are shown in Table 2.

The flow and condensation processes of neon inside circular tubes with inner diameters of 1 mm and 2 mm are numerically simulated for mass fluxes ranging from 20 to 187 kg/(m^2·s). The radial thickness of the first layer of near-wall meshes is every important for flow condensation numerical simulation. The distance to the nearest wall is usually evaluated by the non-dimensional distance (y^+). The formulation shows as follow:

$$y = \frac{y^+ \mu}{\rho u^*} \tag{14}$$

where y^+ is non-dimensional distance, u^* is the friction velocity at the nearest wall, y is the distance to the nearest wall and μ is the local viscosity of the fluid.

In present work, the SST κ-ω model was used to capture turbulence characteristics in the near-wall region. The value of y^+ is usually set as 1 for SST κ-ω model. The radial thickness of the first layer of near-wall mesh is calculated by the inlet vapor phase parameters of the maximum mass flux condition. This setup also provides sufficient resolution for near-wall liquid film flows and smaller mass fluxes. When the saturation is 34.5 K, the calculation thickness of the first layer of near-wall meshes is about 1.2 μm for mass flux 187 kg/(m^2·s). In order to meet the requirements of calculation accuracy, and reduce the calculation workload as much as possible, the radial thickness of the first layer of near-wall meshes set within 1–2 μm in current simulation, while the central area of the cross-section is relatively rough, with a range of 50–100 μm.

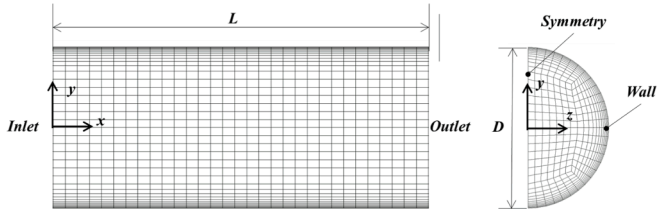

Fig. 1. The representation of the computational domain and the grid configuration.

To ensure smooth progress of the working fluid condensation during the experiment, the wall needs to maintain sufficient subcooling. In the neon flow condensation experiments conducted by Qi et al [17], the condensation test section is designed as the heat flux control condition. Therefore, a constant heat flux condition is adopted for the condensing wall in the model, with the heat flux value set to 7500 W/m^2. The inlet is set to a fully developed velocity condition and the outlet is a pressure outflow boundary condition. The neon vapor at the inlet is saturated with a thermal equilibrium quality of 1. The thermal equilibrium quality is defined as follow.

$$x = \frac{\dot{m}\Delta h - \pi DLq}{\dot{m}\Delta h} \tag{15}$$

where $\dot{m}$ is the mass flow rate, $\triangle h$ is latent heat of evaporation, L is the length from the inlet, q is the heat flux.

3.2. Grid verification

For computational fluid dynamics, the size of the mesh is a critical factor in the accuracy of the simulation results. Theoretically, the smaller the grid scale is, the higher the accuracy of the calculation results, yet the greater the consumption of computational resources and time. Therefore, grid verification is required to ensure the accuracy of calculation and reduce the consumption of computing resources. Toward this goal, the heat transfer coefficients at different grid scales were obtained for condensation flow with a mass flux of 187 kg/(m^2·s) and saturation temperature of 37.5 K. Because the axial velocity gradient of the working fluid flow condensation in a horizontal tube is greater than that of the radial and circumferential gradients, the grid is refined along the axial direction while ensuring that the cross-sectional grid topology remains unchanged. Fig. 2 compares the time averaged local condensation heat transfer values as given by simulation and experiment [17], for different grid configurations. With an increase in the number of computational grids, the calculated condensation heat transfer coefficient gradually approaches a stable value, as shown in Fig. 2(a). Although there is a slight increase in the condensation heat transfer coefficient for certain quality when the grid number reaches 1.38 million, it does not significantly affect the overall trend towards stability. This might be attributed to the finer grid refinement, which allows the Volume of Fluid (VOF) interface reconstruction algorithm to capture smaller suspended liquid droplets. The corresponding discussion also was reported by Zhang et al. [34]. They point out that the more refined grid result in smaller droplets being captured, causing the simulation results to deviate from the actual experiment. To some extent, which might reduce the thickness of the liquid film near the wall. As the condensation heat transfer coefficient is sensitive to the thickness of the liquid film, the reduction in film thickness leads to a slight increase in the local heat transfer coefficient. Furthermore, Fig. 2(b) presents the relative errors between the simulated values and experimental values for different grid numbers. The relative error is defined as the difference between the simulated and experimental values divided by the experimental value. As shown in Fig. 2(b), when the grid number reaches 680,000, the relative errors for moisture content 0.91, 0.4, and 0.13 are 4.8%, 6.9%, and 11.1%, respectively. With increasing grid numbers, the relative errors between the simulated values and experimental values for different moisture contents do not exhibit significant variations. Based on the above analysis, to manage computational costs, grid sizes from 1 μm to 100 μm (corresponding to 680,000 cells) were used for subsequent simulations, with the cross-sectional topology remaining unchanged.

Table 2
Thermophysical properties of the working fluid.

Working fluid	T_{sat} (℃)	P_{sat} (MPa)	ρ_l (kg/m^3)	ρ_v (kg/m^3)	μ_l (μPa.s)	μ_v (μPa.s)	k_l (mW/m•K)	k_v (mW/m•K)	Δh (kJ/kg)	σ (mN/m)
Ne	34.5	0.588	1056.40	50.20	61.454	6.157	111.24	10.337	72.630	2.439
Ne	37.5	0.994	977.92	86.40	48.489	6.996	93.156	12.615	63.898	1.555
N_2	−173.15	0.778	689.353	31.961	75.758	7.429	100.112	10.726	160.975	4.086
R134a	40	0.933	1159.920	45.786	168.037	12.219	76.063	15.081	166.302	6.509
FC-72	57.3	0.102	1557.8	13.38	421.93	11.884	62.579	13.026	84.420	8.178

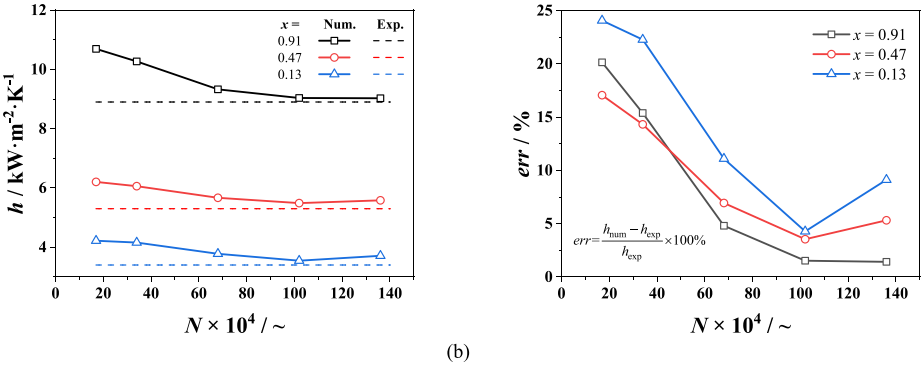

Fig. 2. Comparison of the heat transfer coefficient of condensation inside the tube for different grid densities. (a) The comparison between simulation and experiment results (the dashed lines in the figure are the experimental heat transfer coefficients for specific qualities). (b) The relative errors relative errors between the numerical and experimental values.

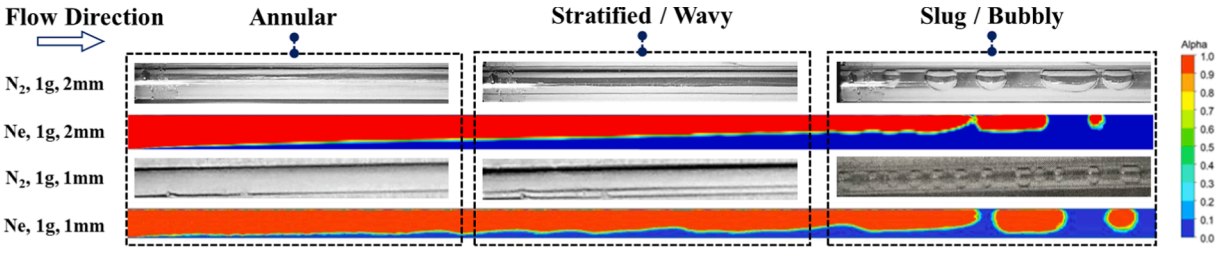

Fig. 3. Flow regime comparison between simulation and experiment.

3.3. Flow pattern comparison between simulation and experiments

Utilizing the aforementioned grid, a simulation analysis was conducted to investigate the condensation flow of neon within the 1 mm and 2 mm diameter pipes at a mass flux of 20 kg/(m^2·s), to yield flow patterns of the condensation process. The two-phase flow pattern during condensation is depicted in Fig. 3, revealing predominantly annular flow, wavy/stratified flow, and slug/bubbly flow. Due to the strict requirements of environmental temperature and experimental materials for visualizing two-phase flow patterns under deep cryogenic conditions, no flow pattern maps have been reported previously for neon condensation in microtubes. In this study, the nitrogen condensation flow pattern observation results obtained by Qi [17] were employed for comparison. Fig. 3 presents the nitrogen flow pattern under a mass flux condition of 20–40 kg/(m^2·s) in 1 mm and 2 mm diameter tubes. By comparing the experimental flow patterns, it can be seen that the main flow patterns of the nitrogen working fluid are annular flow, stratified flow, and slug flow for the 2 mm diameter tube. The simulated flow pattern of neon condensation is the same as that of nitrogen, except that the thickness of the liquid film at the bottom of the tube under bubble flow seems to be thicker. For the 1 mm diameter tube, the flow pattern of nitrogen is still dominated by annular flow, stratified flow, and bubble flow, but the simulated condensation flow pattern of neon shows a more obvious wavy stratified flow. In addition, the condensation tail bubbles of nitrogen in the experiment exhibit a symmetric distribution along the middle plane of the pipe, while the axial center of the condensation tail bubbles of neon is clearly offset toward being further upward in the tube. This indicates that the gravity effect may present a more significant influence on the flow pattern of neon condensation, which may be attributed to the surface tension of neon being smaller than that of nitrogen (Table 2). Nevertheless, the flow pattern obtained from the simulation of neon condensation is consistent with the observation results of the nitrogen condensation flow pattern, which somewhat verifies the rationality of the current model.

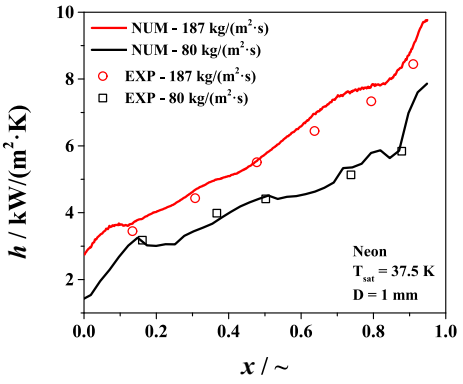

Fig. 4. Comparison of the heat transfer coefficients between simulation and experiment.

4. Results and discussion

4.1. Influence of mass flux on flow condensation

Fig. 4 shows a comparison between the simulation and experimental results [17] of the condensation heat transfer coefficient in a 1 mm tube under different mass flux conditions. The saturation temperature is 37.5 K and the inlet working fluid is saturated vapor. It should be noted that the quality value in the experimental test is defined as the average value of the thermal equilibrium quality at the inlet and outlet of the test section. In the experimental test, because the difference between the wall temperature and the saturation temperature working fluid is very small, the variation difference between the quality of the condensation outlet and the inlet of the test section is also small. Therefore, the test section average quality is very closed to the actual quality, which can be used to analyze the condensing heat transfer coefficient. Shown as Fig. 4, The simulated and experimental results under different working conditions are relatively similar and show high consistency, which verifies the reliability of the model. In addition, as shown in Fig. 4, the condensation heat transfer coefficient of the neon is primarily influenced by the mass flux and vapor quality, which affect the distribution and motion of the wall condensate film. In fact, the intensity of condensation heat transfer depends mainly on the distribution and motion of the wall condensate film. A lower vapor quality leads to higher liquid holdup in the cross section, which increases the average thickness of the cross-sectional liquid film, resulting in a smaller condensation heat transfer coefficient. On the other hand, increasing the inlet mass flux improves the velocity of the two-phase flow, the interfacial shear velocity between the vapor and liquid phases, and the interfacial convective heat transfer between the two phases. This, in turn, improves the heat transfer efficiency, particularly when the liquid film enters the turbulent state. Additionally, when the interfacial velocity between the vapor and liquid phases reaches a certain value, the interfacial shear effect becomes more significant. A notable feature is that this effect drives the formation of a wavy liquid film while reducing the thickness of the wall liquid film, thereby improving the condensation heat transfer efficiency.

To analyze the effects of the vapor quality and mass flux on the distribution and thickness of the liquid film, Fig. 5 shows the circumferential thickness of the wall liquid film as a function of the mass flux and vapor quality. Under the same mass flux conditions, the analysis of the cross-sectional liquid film distribution shows that gravity affects the distribution of the neon working fluid condensation film in a 1 mm tube. Under the action of gravity, the top condensation film moves toward the bottom of the cross section, forming a thicker liquid film at the bottom of tube, as shown in Fig. 5. As the quality decreases, it becomes noticeable that the liquid film at the bottom of tube significantly thickens, while the change in thickness of the top liquid film remains relatively small. In some range ($\theta = 10°–40°$), there may even be instances where the top liquid film thickness under low quality conditions is smaller than that under high quality conditions. However, it is important to note that this thinning of the top liquid film has a negligible influence on the local condensation heat transfer coefficient, especially when compared to the significant increase in thickness of the bottom liquid film. Similarly, from the liquid film distribution graph, it can be seen that under the same vapor quality conditions, increasing the mass flux reduces the thickness of the wall liquid film, which is more evident at high vapor quality. Furthermore, comparing the circumferential liquid film thicknesses under a vapor quality of 0.7 and when θ is greater than 110°, the liquid film thickness under high mass flux conditions is significantly smaller.

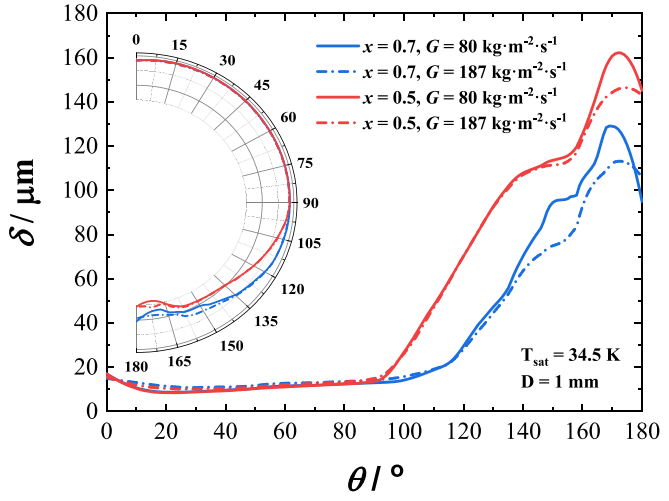

Fig. 5. The effect of mass flux on the distribution of the cross-sectional condensate film.

4.2. The effects of tube diameter on flow condensation

Fig. 6 presents a comparison of the condensation heat transfer coefficients of the neon working fluid in 1 mm and 2 mm diameter tubes under a mass flux of 20 kg/(m^2·s). The results indicate that the heat transfer coefficient is significantly affected by the tube diameter, with smaller diameters enhancing the condensation heat transfer. Specifically, at the corresponding most vapor quality range, the heat transfer coefficient in the 1 mm diameter tube is higher than that in the 2 mm diameter tube, as shown in Fig. 6. This occurs mainly because under the influence of gravity, the condensate film moves downward along the tube wall, forming a thicker liquid film at the bottom of the tube. As the tube diameter increases, the effect of gravity becomes more pronounced, resulting in a thicker liquid film at the bottom and lower condensation heat transfer efficiency. Additionally, the heat transfer coefficient in the 1 mm diameter tube exhibits a significant increase and sharp decrease in the low vapor quality region, which is similar to the findings of Wu et al. [35] and is more pronounced in their simulation, which used a 0.1 mm diameter tube. This occurs mainly due to the strong transient effect of liquid bridge-plug-bubble detachment during the transition from annular flow to slug flow. The formation of a liquid bridge implies the presence of a bubble plug, which significantly enhances the condensation heat transfer in the thin liquid film region between the bubble plug and the tube wall. However, as the condensation process continues, the bubble plug gradually condenses into a small bubble that is enveloped by the mainstream liquid, resulting in a decrease in the condensation heat transfer coefficient. As shown in Fig. 6, as the vapor quality further decreases, the condensation heat transfer coefficient in the 2 mm diameter tube is slightly higher than that in the 1 mm diameter tube. This is also due to the strong transient effect of bubble detachment and condensation at the end of condensation, but at this condition, the lower

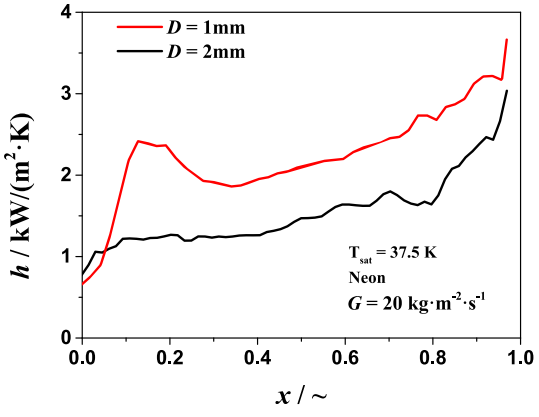

Fig. 6. The effect of the tube diameter on the condensation heat transfer.

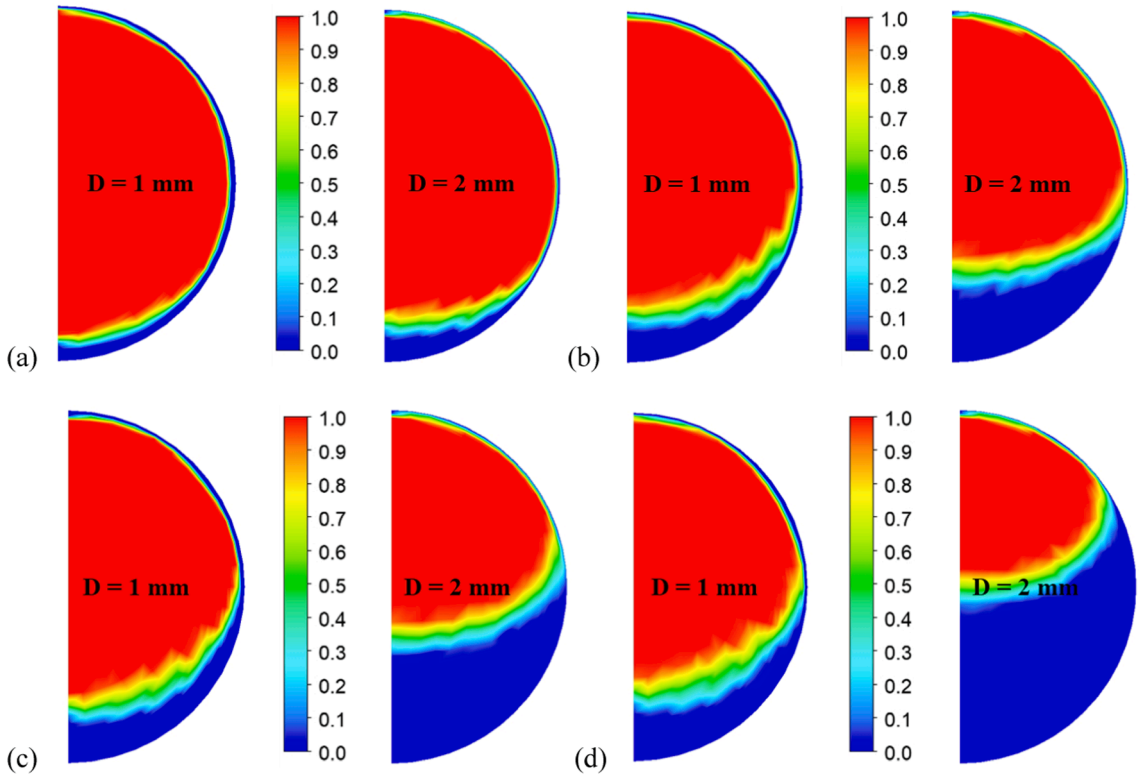

Fig. 7. Distribution of the cross-sectional area of the condensate film for different quality for diameter 1 mm and 2 mm. (a) $x = 0.9$; (b) $x = 0.7$; (c) $x = 0.5$; (d) $x = 0.3$.

vapor quality induces the deteriorating condensation heat transfer process.

To analyze the effect of the tube diameter on the vapor–liquid distribution in the condensation flow, Fig. 7 shows the cross-sectional distribution of the liquid film under different tube diameters varying with the vapor quality. For the same tube diameter, the liquid film thickness at the bottom the tube cross section is obviously thicker than the top under the gravity effect. As the quality gradually decreases, the thickness of the bottom liquid film further increases, forming the bottom thick liquid film or "liquid pool". This trend is more obvious for the larger tube diameter. For the same quality, the proportion of the liquid film at the bottom of the larger diameter tube is significantly higher than that of the smaller diameter tube. Further analysis reveals that under equal mass flux conditions, the *Bo* (Bond number) and maximum superficial gas *Fr* (Froude number) of the 1 mm diameter tube are 5.62 and 0.73, respectively, while those of the 2 mm diameter tube are 22.49 and 0.51, respectively. According to the gravity independence criterion proposed by Zhao et al. [36], expressed as follow:

$$\begin{cases} Bo = (\rho_l - \rho_v)gD^2/\sigma \leqslant Bo_{cr} \approx 1.5 - 6 \\ Fr = U_{sg}/\sqrt{(\rho_l - \rho_v)gD/\rho_v} \geqslant Fr_{cr} \approx 0.54 - 2.2 \end{cases} \tag{14}$$

where U_{sg} is superficial gas velocity. The critical range of the *Bo* number is 1.56–6, and the critical range of the superficial gas *Fr* number is 0.54–2.2.

In the current simulation, the 1 mm diameter tube is located at the upper boundary of the gravity-independent transition zone and is closer to the gravity-dominated region, while the *Bo* number of the 2 mm diameter tube is in the gravity-dominated region and the *Fr* number is at the lower boundary of the critical range, close to the gravity-dominated region. Therefore, the influence of gravity on the liquid film distribution is more pronounced in the 2 mm diameter tube.

4.3. The effects of gravity on flow condensation

As noted in the previous section, the flow and heat transfer performance of two-phase flow mainly depend on the coupled effects of inertia, surface tension, and gravity within the system. Compared with other working fluids, such as R134a and FC-72, as shown in Table 2, neon shows a significantly lower surface tension. For the low surface tension of the neon working fluid, even under the condition of a 1 mm tube diameter, the effect of gravity on the condensation flow is still significant. This section mainly focuses on the influence of gravity level on the condensation flow and heat transfer characteristics of neon, including zero gravity, Lunar gravity (0.17 g_e), Martian gravity (0.38 g_e), and Earth gravity (1 g_e). In the simulation, the direction of gravity is perpendicular to the flow direction of the working fluid in the horizontal tube.

4.3.1. The effects of gravity on the condensation flow pattern

According to previous research results, the effect of gravity on condensation flow and heat transfer performance mainly occurs under conditions of lower mass flux and lower vapor quality. Fig. 8 compares the influence of gravity level on the condensation flow pattern under a mass flux of 20 kg/(m^2·s). As analyzed earlier, under normal gravity level, the condensation flow pattern mainly includes annular flow, wavy stratified flow, and slug flow. As the gravity level decreases, the annular flow region gradually expands and changes from eccentric annular flow to concentric annular flow, and more small ripples can be observed on the surface of the annular flow. This phenomenon is consistent with the observation results of microgravity condensation flow patterns conducted by Berto et al. [14] in a parabolic flight microgravity experiment, which showed that under normal gravity conditions, the annular flow corresponds to a smooth surface, while under microgravity conditions, more small ripples appear on the surface of the annular flow. One possible reason for this phenomenon is that the decrease in gravity level weakens the interface stability that is originally maintained by surface

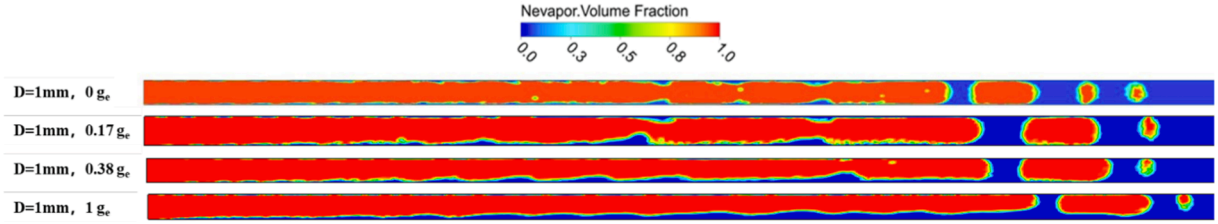

Fig. 8. The condensation flow pattern for different gravity levels (G = 20 kg/(m^2·s)).

tension and gravity, leading to an increase in shear instability at the vapor–liquid interface. In addition, due to the weakening of the driving effect of gravity on the circumferential liquid film, the thickness of the liquid film at the bottom of the circular tube is significantly reduced, and the surface wave of the liquid film formed under gravity is more significant. A more important observation is the change from fine ripples under normal gravity level to larger wave packets, although there are also clear areas of thin liquid film between the wave packets, and the thickness of the thin liquid film decreases as the gravity level decreases.

Gravity level also have an effect on the formation and movement of condensation vapor plugs and tail bubbles. Under normal gravity level, the condensation vapor plug shows a thicker liquid film at the bottom, while as the gravity level decreases, the liquid film at the bottom gradually thins, and the condensation vapor plug under zero gravity level is close to the tube wall. Furthermore, the condensation tail bubbles are also sensitive to gravity level, and under normal gravity level, they are located at the upper part of the tube wall and a thin liquid film area resides at the top, but as the gravity level decreases, the position of the condensation tail bubbles gradually shifts toward the center of the tube, and the liquid film between the condensation tail bubbles and the tube wall increases. It should be noted that liquid droplet entrainment occurs in the tube under zero gravity level, which did not occur in the normal gravity simulation under the same operating conditions. This may occur due to the low surface tension of the neon working fluid, which reduces the stability of the vapor–liquid interface under the same mass flux condition. However, the occurrence of the droplet entrainment phenomenon will reduce the thickness of the circumferential liquid film to a certain extent.

4.3.2. *The effects of gravity on the local liquid film distribution*

To analyze the effect of gravity on the distribution of the liquid film in condensation flow, Fig. 9 shows the cross-sectional liquid film distribution under different mass flux and quality. To avoid the influence of transient effects on the analysis results, time-averaged interface position data corresponding to a period of time after the condensation flow is stabilized are used for analysis. Under the same mass flux conditions, for interfaces with higher quality, the circumferential liquid film distribution is more uniform, with only a relatively thin bottom liquid film under normal gravity level. As the gravity level decreases, the circumferential liquid film distribution becomes even more uniform. As the cross-sectional quality decreases, the influence of gravity on the distribution of the cross-sectional liquid film becomes more significant. Specifically, under the action of gravity, the bottom liquid film is thickened as the quality decreases, and the difference in liquid film thickness under different gravity levels becomes more pronounced, as shown in Fig. 9(c) and 9(d). The influence of mass flux on the distribution of the cross-sectional liquid film is mainly reflected in the change in the distribution shape. When the vapor quality is high, increasing the mass flux does not significantly change the time-averaged liquid film distribution along the cross-section, as shown in Fig. 9(a) and 9(d). However, for cross-sections with lower quality, increasing the mass flux will simultaneously increase the circumferential liquid film fluctuation amplitude and the circumferential area of the interface, as shown in Fig. 9(e) and 9 (f). Overall, gravity has a pronounced effect on the distribution of the cross-sectional liquid film, especially for cross-sections with lower vapor quality, which is manifested in the significant thickening of the bottom liquid film with increasing gravity level. This occurs because the mechanism of gravity-driven condensation liquid film movement toward the bottom is accompanied by the presence of gravity and is not obscured by other factors, and the driving effect of gravity on the liquid film only changes when the gravity level or direction changes.

4.3.3. *The effects of gravity on the condensation heat transfer coefficient*

Fig. 10 shows the effect of gravity level on the local heat transfer coefficient during condensation for different vapor qualities at a mass flux of 40 kg/(m^2·s). Similarly, the analyzed local heat transfer coefficient represents the time-averaged value on a fixed cross-section. The image shows that the gravity level has an apparent impact on the local heat transfer coefficient. Under zero gravity level, there is no significant difference in the circumferential distribution of the local heat transfer coefficient. However, as the vapor quality of the cross-section decreases, the local heat transfer coefficient shows a decreasing trend. This is because the condensate film is circumferentially distributed uniformly and the film thickens as the vapor quality decreases under zero gravity level. As the gravity level increases, the circumferential asymmetry of the local heat transfer coefficient becomes evident, with stronger asymmetry as the gravity level increases, as shown in Fig. 10(b).

To analyze the impact of gravity variations on the condensation heat transfer, the heat transfer coefficient corresponding to normal gravity level can serve as a baseline. When the condensation heat transfer coefficient under certain gravity level is higher than that under normal gravity, it is referred to as gravity enhancement condensation heat transfer. Conversely, if the coefficient is lower, it is termed gravity deterioration condensation heat transfer. When the two coefficients are equal, it indicates gravity independence condensation heat transfer. Building upon this understanding, further investigation can be conducted to explore the mechanisms underlying the effects of gravity variations on the intensity of condensation heat transfer.

As shown in Fig. 10, the circumferential asymmetry of the local heat transfer coefficient induced by the increase in gravity level is mainly induced by the decrease of the condensation heat transfer coefficient in the bottom liquid film region and the resulting enhancement of the heat transfer in the top liquid film region. In the bottom liquid film region, an increase in gravity level leads to a significant decrease of the condensation heat transfer coefficient. Conversely, an increase in gravity level also significantly enhances the condensation heat transfer in the top liquid film region. This implies a certain competitive relationship between the decrease of the condensation heat transfer in the bottom liquid film region and the enhancement of the heat transfer in the top liquid film region induced by the change in gravity level. When the deterioration of the condensation in the bottom liquid film region dominates, the cross-section exhibits deteriorated condensation heat transfer with an increase in gravity level. Otherwise, when the enhancement of the heat transfer in the top liquid film region dominates, the cross-section exhibits enhanced condensation heat transfer with an increase in gravity level.

The variation in the flow condensation heat transfer coefficient with respect to vapor quality under different mass flux and gravity levels is presented in Fig. 11. Overall, the condensation heat transfer coefficient decreases with decreasing vapor quality. For a mass flux of 20 kg/(m^2·s),

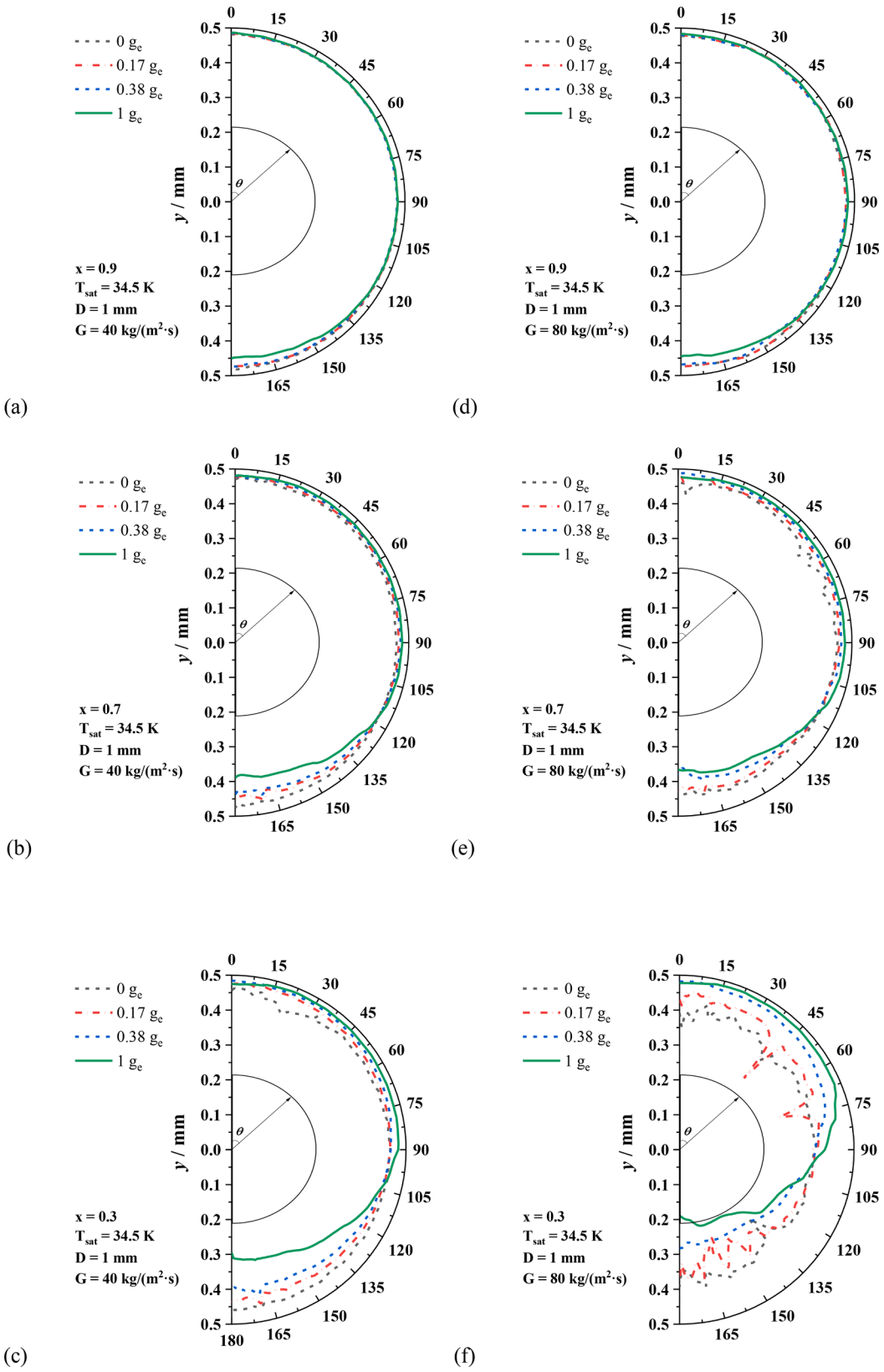

Fig. 9. The gravity effects on the cross-section condensate film distributions under different conditions. (a) G = 40 kg/(m^2·s), x = 0.9. (b) G = 40 kg/(m^2·s), x = 0.7. (c) G = 40 kg/(m^2·s), x = 0.3. (d) G = 80 kg/(m^2·s), x = 0.9. (e) G = 80 kg/(m^2·s), x = 0.7. (f) G = 80 kg/(m^2·s), x = 0.3.

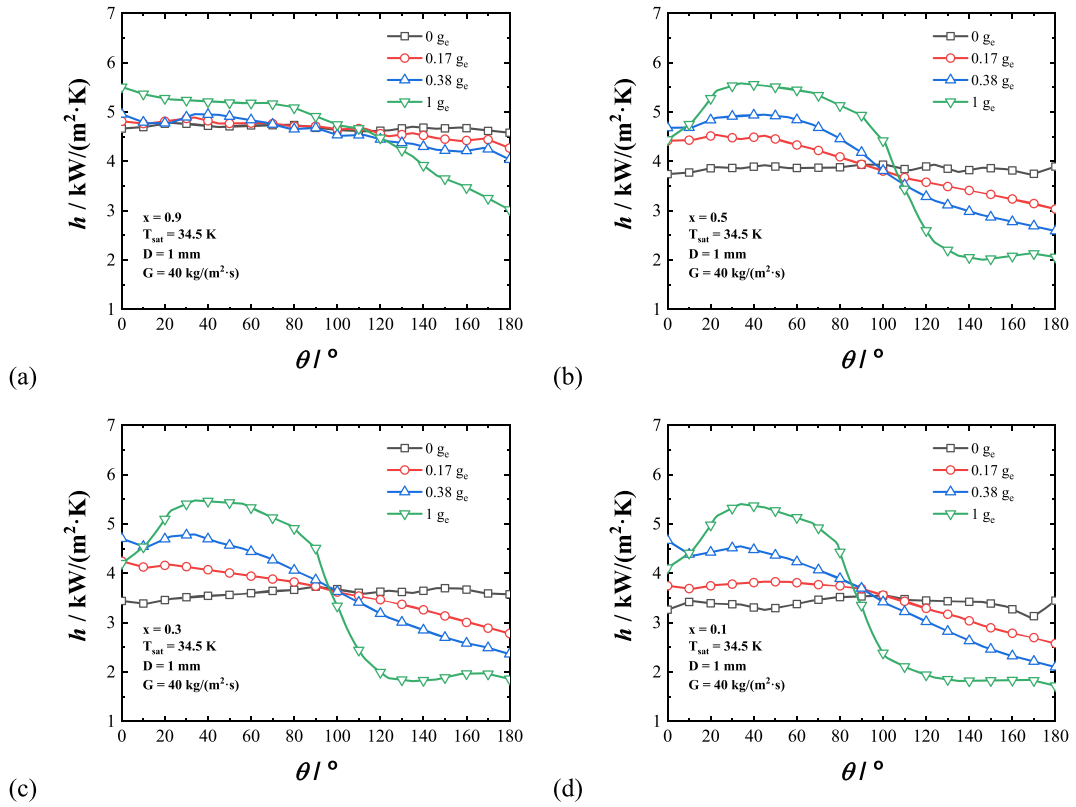

Fig. 10. The time-averaged local heat transfer coefficients of different qualities at a mass flux of 40 kg/(m^2·s) for different gravity levels.

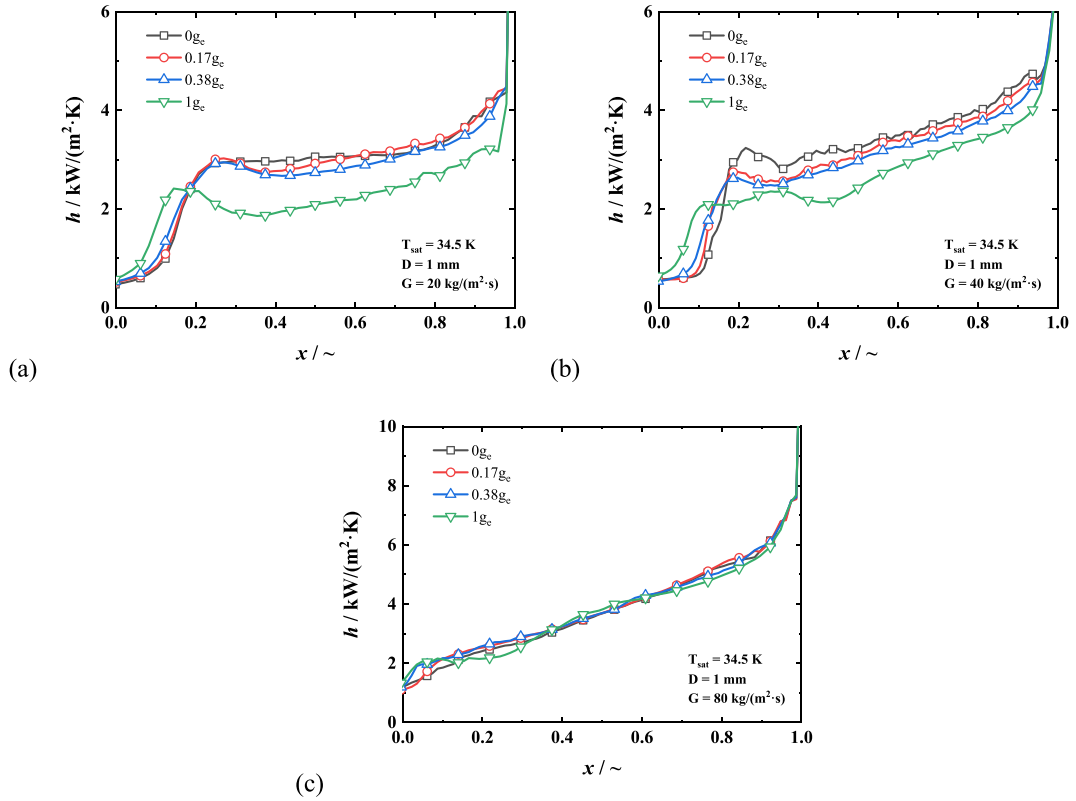

Fig. 11. Time-averaged condensation heat transfer coefficients for different gravity levels. (a) G = 20 kg/(m^2·s). (b) G = 40 kg/(m^2·s). (c) G = 80 kg/(m^2·s).

the condensation heat transfer coefficient exhibits gravity independence within the vapor quality larger than 0.98. This vapor quality range corresponds to the vapor inlet section, where the vapor directly contacts the wall and condenses to form a uniform thin liquid film along the circumference. Within the range of 0.98–0.19, the zero gravity condensation heat transfer coefficient is higher than that of normal gravity, indicating an enhancement of condensation heat transfer under zero gravity level in the current operating conditions, as shown in Fig. 11(a). Within the vapor quality range below 0.19, the zero gravity condensation heat transfer coefficient is lower than that of normal gravity, indicating a deterioration of condensation heat transfer under zero gravity level. The same trend can also be observed under a mass flux condition of 40 kg/(m^2·s). However, there are some changes in the quality ranges corresponding to different gravity effects. The quality ranges for gravity independence, gravity deterioration heat transfer, and gravity-enhanced heat transfer are larger than 0.96, 0.96–0.16, and less than 0.16, respectively, shown as Fig. 11(b). The increase in condensation heat transfer under zero gravity level seem inconsistent with previous experimental results [14]. However, the gravity effect on condensation flow depends mainly on the mass flux and quality. Thus, similar reports have been found in previous studies, such as Wen et al. [22], who also found that the gravity level change can both enhance and deteriorate condensation heat transfer in R1234ze(E) horizontal tube flow condensation simulations. In fact, the heat transfer and fluid flow characteristics during the condensation process are highly sensitive to the distribution and transport behavior of the condensate, directly affecting the local liquid film thickness and heat transfer intensity.

Therefore, the possible enhancement of condensation heat transfer under zero gravity level may be based on the following facts. On the one hand, gravity level significantly alters the vapor–liquid distribution on the tube cross-section, affecting the local heat transfer coefficient. For the same void fraction interface, under normal gravity, the gravitational force drives the top liquid flow toward the bottom of the tube, resulting in a thin top liquid film and an eccentric circular interface with a thick bottom liquid film, which shows a trend of enhanced heat transfer. Under zero gravity level, the interface is less constrained by gravity and is more likely to form interface waves, increasing the interface heat transfer area and showing a trend of enhanced heat transfer under zero gravity environments. In fact, from the perspective of the liquid film distribution on the cross-section, the impact of gravity level on the heat transfer coefficient is the result of the competing effects of the two aforementioned mechanisms.

On the other hand, gravity can alter the stability of the vapor–liquid interface during the condensation process under the coupling effect of flow and heat transfer inside the tube. Inertial force, gravity, and surface tension are important forces in the condensation flow, and changes in local stresses at the interface can significantly alter the interface shape. For tube flow, the instability of the interface mainly stems from Rayleigh-Taylor instability (caused by the density difference between vapor and liquid) and Kelvin-Helmholtz instability (caused by the velocity difference between vapor and liquid) [37]. The aforementioned instability phenomena exist during the condensation process and can increase the interface fluctuation and even cause droplet entrainment, which can increase the cross-sectional area and reduce the thickness of the liquid film near the wall, thus enhancing heat transfer. This has been discussed in the previous section on the effect of gravity on the condensation flow pattern. Under zero gravity level, the vapor–liquid interface becomes more prone to instability, with significant fluctuations and droplet entrainment at the cross section, thereby enhancing the condensation heat transfer. Comparing the simulation flow patterns, it can be observed that the interface stability is difficult to maintain under zero gravity level, with significant droplet entrainment, whereas under normal gravity level, the interface is more stable and smoother.

In addition, it is worth noting that as the mass flux increases, the influence of gravity on the condensation heat transfer coefficient appears to gradually weaken. When the mass flux reaches a certain level, the effect of gravity on the condensation heat transfer coefficient is insignificant, as shown in Fig. 11(c). It can be seen from Fig. 11(c) that in the current simulation, when the mass flux reaches 80 kg/(m^2·s), the condensation heat transfer coefficients under different gravity levels are very similar. This indicates that increasing the inlet gas phase velocity or mass flux of the condensation flow may be an effective way to suppress the effect of gravity on the condensation heat transfer coefficient. Similar viewpoints have been mentioned in the studies of O'Neill et al. [7] and Berto et al. [14]. However, it should be noted that the increase in mass flux can only effectively suppress the effect of gravity in the higher vapor quality range. For the lower quality region, the trend of deteriorating condensation heat transfer due to the decrease in gravity is not completely suppressed. Therefore, in the design of the condenser, attention should be given to the effect of gravity on condensation heat transfer in low-quality regions under operating conditions. In summary, the influence of gravity on the condensation flow is directly related to the condensation flow state. Therefore, analyzing the influence of gravity on condensation flow requires consideration of specific operating conditions.

5. Conclusions

A three-dimensional transient simulation model of neon flow condensation was established and simulated based on the VOF model. The mesh independence of the model was analyzed, and the model was validated by comparing the flow pattern and heat transfer coefficients to experimental results. Using the validated model, the effects of mass flux, tube diameter, and gravity on the condensation flow and heat transfer performance were simulated and analyzed. The main research findings of this study are summarized as follows:

(1) Mass flux has a significant effect on the condensation heat transfer coefficient. As the mass flux increases, the heat transfer coefficient of the flow condensation also increases. For cryogenic working fluids, small tube diameters enhance condensation heat transfer, and the effect of gravity on the condensation flow pattern remains significant even in small diameter tubes.
(2) Due to the low surface tension of neon, the interface of liquid film stability is weak during condensation flow, especially under zero gravity level. With the decrease of the gravity level, the vapor–liquid interface is more prone to become unstable and form interface waves or even result in droplet entrainment.
(3) Gravity can both enhance and deteriorate heat transfer depending on the result of the competition between the inertial force, surface tension, and gravity in the flow and heat transfer process. For neon condensation under lower mass flux, decreasing the gravity level enhances condensation heat transfer. However, in the lower vapor quality region, decreasing gravity level leads to deteriorated condensation heat transfer.
(4) Increasing the mass velocity of the condensation flow can partially suppress the effects of gravity on heat transfer. However, this is only effective for condensation processes within a higher quality range. For the low quality range, such as slug flow and bubbly flow regions, the effect of gravity remains significant, and decreasing the gravity level deteriorates condensation heat transfer.

Declaration of Competing Interest

The authors declare that they have no known competing financial interests or personal relationships that could have appeared to influence the work reported in this paper.

Data availability

Data will be made available on request.

Acknowledgments

This work was supported by the National Natural Science Foundation of China (No. 11972040) and National Key Research and Development Program of China (No. 2022YFF0503502).

References

[1] I. Mudawar, Flow boiling and flow condensation in reduced gravity, Adv. Heat Transf. 49 (2017) 225–306, https://doi.org/10.1016/bs.aiht.2017.06.002.
[2] K. El Kadi, F. Alnaimat, S.A. Sherif, Recent advances in condensation heat transfer in mini and micro channels: a comprehensive review, Appl. Therm. Eng. 197 (2021), 117412, https://doi.org/10.1016/j.applthermaleng.2021.117412.
[3] B.X. Wang, X.Z. Du, Study on laminar film-wise condensation for vapor flow in an inclined small/mini-diameter tube, Int. J. Heat Mass Transf. 43 (2000) 1859–1868, https://doi.org/10.1016/S0017-9310(99)00256-2.
[4] S. Lips, J.P. Meyer, Experimental study of convective condensation in an inclined smooth tube. Part I: Inclination effect on flow pattern and heat transfer coefficient, Int. J. Heat Mass Transf. 55 (2012) 395–404, https://doi.org/10.1016/j.ijheatmasstransfer.2011.09.033.
[5] S. Bortolin, G.E. Achkar, M. Kostoglou, et al., Experimental investigations on condensation in the framework of ENhanced COndensers in microgravity (ENCOM-2) project, Microgravity Sci. Technol. 26 (2014) 335–349, https://doi.org/10.1007/s12217-014-9402-0.
[6] I. Park, L.E. O'Neill, C.R. Kharangate, I. Mudawar, Assessment of body force effects in flow condensation, Part I: Experimental investigation of liquid film behavior for different orientations, Int. J. Heat Mass Transf. 106 (2017) 295–312, https://doi.org/10.1016/j.ijheatmasstransfer.2016.05.065.
[7] L.E. O'Neill, I. Park, C.R. Kharangate, V.S. Devahdhanush, V. Ganesan, I. Mudawar, Assessment of body force effects in flow condensation, part II: Criteria for negating influence of gravity, Int. J. Heat Mass Transf. 106 (2017) 313–328, https://doi.org/10.1016/j.ijheatmasstransfer.2016.07.019.
[8] L.E. O'Neill, R. Balasubramaniam, H.K. Nahra, M.M. Hasan, I. Mudawar, Flow condensation heat transfer in a smooth tube at different orientations: Experimental results and predictive models, Int. J. Heat Mass Transf. 140 (2019) 533–563, https://doi.org/10.1016/j.ijheatmasstransfer.2019.05.103.
[9] O. Lebaigue, C. Colin, A. Larue de Tournemine, Forced convection boiling and condensation of ammonia in microgravity, in: 13rd Int. Heat Transfer Conf., Sydney, Australia, 13-18 August 2006. MPH-25. https://doi.org/10.1615/IHTC13.p12.250.
[10] H. Kawasaki, A. Okamoto, R. Hatakenaka et al., Condenser of reservoir embedded loop heat pipe under orbital environment, in: 5th Int. Topical Team Workshop on Two-phase Systems for Ground & Space Applications, Kyoto, Japan, September 26-29, 2010.
[11] H. Lee, I. Mudawar, M.M. Hasan, Experimental and theoretical investigation of annular flow condensation in microgravity, Int. J. Heat Mass Transfer 61 (2013) 293–309, https://doi.org/10.1016/j.ijheatmasstransfer.2013.02.010.
[12] H. Lee, I. Park, C. Konishi, I. Mudawar, R.I. May, J.R. Juergens, J.D. Wagner, N.R. Hall, H.K. Nahra, M.M. Hasan, J.R. Mackey, Experimental investigation of flow condensation in microgravity, J. Heat Transfer 136 (2014) 021502-1–11. https://doi.org/10.1016/j.ijheatmasstransfer.2013.02.010.
[13] M. Azzolin, S. Bortolin, L.P.L. Nguyen, P. Lavieille, A. Glushchuk, P. Queeckers, M. Miscevic, Carlo Saverio Iorio, Davide Del Col, Experimental investigation of in-tube condensation in microgravity, Int. Commun. Heat Mass Transf. 96 (2018) 69–79, https://doi.org/10.1016/j.icheatmasstransfer.2018.05.013.
[14] A. Berto, M. Azzolin, P. Lavieille, A. Glushchuk, P. Queeckers, S. Bortolin, Carlo Saverio Iorio, Marc Miscevic, Davide Del Col, Experimental investigation of liquid film thickness and heat transfer during condensation in microgravity, Int. J. Heat Mass Transfer 199 (2022), 123467, https://doi.org/10.1016/j.ijheatmasstransfer.2022.123467.
[15] C. Qi, X.T. Chen, W. Wang, J.Y. Miao, H.X. Zhang, Experimental investigation on flow condensation heat transfer and pressure drop of nitrogen in horizontal tubes, Int. J. Heat Mass Transf. 132 (2019) 985–996, https://doi.org/10.1016/j.ijheatmasstransfer.2018.11.092.
[16] C. Qi, X.T. Chen, W. Wang, J.Y. Miao, H.X. Zhang, Experiment and simulation on downward flow condensation of nitrogen in vertical tubes, Int. J. Heat Mass Transf. 146 (2020) 118827, https://doi.org/10.1016/j.ijheatmasstransfer.2019.118827.
[17] Q. Chao, Investigation on Flow and Heat Transfer Characteristics of Condensation in Tubes for Nitrogen and Neon, Shanghai Jiao Tong University, Shanghai, 2019 in Chinese.
[18] C.R. Kharangate, I. Mudawar, Review of computational studies on boiling and condensation, Int. J. Heat Mass Transf. 108 (2017) 1164–1196, https://doi.org/10.1016/j.ijheatmasstransfer.2016.12.065.
[19] E. Da Riva, D. Del Col, Effect of gravity during condensation of R134a in a circular minichannel, Microgr. Sci. Technol. 23 (2011) 87–97, https://doi.org/10.1007/s12217-011-9275-4.
[20] Da Riva E., Del Col D., Cavallini A, et al., Simulation of Condensation in a Circular Minichannel: Application of VOF Method and Turbulence Model, International Refrigeration and Air Conditioning Conference, 2010, 1160.
[21] W. Li, J.Z. Zhang, P.F. Mi, J.F. Zhao, Z. Tao, R.N.C. Peter, I.P.S. Tom, The effect of gravity on R410A condensing flow in horizontal circular tubes, Numer. Heat Transf. Part A: Applications 3 (2017) 327–340, https://doi.org/10.1080/10407782.2016.1264743.
[22] J. Wen, X. Gu, Y.C. Liu, S.M. Wang, Y.Z. Li, Effect of Surface Tension, Gravity and Turbulence on Condensation Patterns of R1234ze(E) in Horizontal Mini/Macro-Channels, Int. J. Heat Mass Transf. 125 (2018) 153–170, https://doi.org/10.1016/j.ijheatmasstransfer.2018.04.039.
[23] X. Gu, J. Wen, J. Tian, S.M. Wang, J.Y. Tu, Numerical study on condensation annular flow of R1234ze(E) inside an inclined tube, Appl. Therm. Eng. 163 (2019), 114359, https://doi.org/10.1016/j.applthermaleng.2019.114359.
[24] H. Ganapathy, A. Shooshtari, K. Choo, S. Dessiatoun, M. Alshehhi, M. Ohadi, Volume of fluid based numerical modeling of condensation heat transfer and fluid flow characteristics in microchannels, Int. J. Heat Mass Transf. 65 (2013) 62–72, https://doi.org/10.1016/j.ijheatmasstransfer.2013.05.044.
[25] Y.C. Lei, I. Mudawar, Z.Q. Chen, Computational and experimental investigation of condensation flow patterns and heat transfer in parallel rectangular micro-channels, Int. J. Heat Mass Transf. 149 (2020), 119158, https://doi.org/10.1016/j.ijheatmasstransfer.2019.119158.
[26] H.B. Zhong, Z.Y.. Wei, Y. Man, S.W. Pan, J.T. Zhang, B. Niu, Y. Xi, Y. Ouyang, Q. G. Xiong, Prediction of instantaneous yield of bio-oil in fluidized biomass pyrolysis using long short-term memory network based on computational fluid dynamics data, Journal of Cleaner Production 391 (2023), 136192, https://doi.org/10.1016/j.jclepro.2023.136192.
[27] W.X. She, Z.Y. Zuo, H. Zhao, Q. Gao, L.X. Zhang, X.M. Shao, Novel models for predicting the shape and motion of an ascending bubble in Newtonian liquids using machine learning, Phys. Fluids 34 (2022) 043313, doi:10.1063/5.0088942.
[28] C.W. Hirt, B.D. Nichols, Volume of fluid (VOF) method for the dynamics of free boundaries, J. Comput. Phys. 39 (1981) 201–225, https://doi.org/10.1016/0021-9991(81)90145-5.
[29] J.U. Brackbill, D.B. Kothe, C. Zemach, A continuum method for modeling surface tension, J. Comput. Phys. 100 (1992) 335–354, https://doi.org/10.1016/0021-9991(92)90240-Y.
[30] F.R. Menter, Two-equation eddy-viscosity turbulence models for engineering applications, AIAA J. 8 (1994) 1598–1605, https://doi.org/10.2514/3.12149.
[31] W.H. Lee, A Pressure Iteration Scheme for Two-Phase Flow Modeling, Hemisphere Publishing, Washington, 1980.
[32] ANSYS Fluent user's guide, ANSYS Inc, Canonsburg, PA, 2015.
[33] E.W. Lemmon, M.L. Huber, M.O. McLinden, NIST Standard Reference Database23: Reference Fluid Thermodynamic and Transport Properties-REFPROP, Version 9.0, National Institute of Standards and Technology, Standard ReferenceData Program, Gaithersburg, 2010.
[34] C.W. Zhang, Z.Y. Zhang, W. Kun, X. Xia, XJ.. Fan, Atomization ofmisaligned impinging liquid jets, Phys. Fluids 33 (2021), 093311, https://doi.org/10.1063/5.0061981.
[35] C.X. Wu, J.M. Li, Numerical simulation of flow patterns and the effect on heat flux during R32 condensation in microtube, Int. J. Heat Mass Transf. 121 (2018) 265–274, https://doi.org/10.1016/j.ijheatmasstransfer.2017.12.123.
[36] J.F. Zhao, J.C. Xie, H. Lin, W.R. Hu, A.V. Ivanov, A.Yu. Belyaev, Experimental Studies on Two-Phase Flow Patterns aboard the Mir Space Station, Int. J. Multiphase Flow 27 (2001) 1931–1944, https://doi.org/10.1016/S0301-9322(01)00037-4.
[37] C. Bern, A. Escriva, J.L. Munoz-Cobo, L.E. Herranz, Review of droplet entrainment in annular flow: Characterization of the entrained droplets, Progress in Nuclear Energy 79 (2015) 64–86, https://doi.org/10.1016/j.pnucene.2014.11.011.